Journal of Engineering and Sustainable Development
https://jeasd.uomustansiriyah.edu.iq/index.php/jeasd
https://doi.org/10.31272/jeasd.28.3.1

Vol. 28, No. 03, May 2024
ISSN 2520-0917

Original Research

INVESTIGATING BACK SURFACE COOLING SYSTEM USING PHASE CHANGE MATERIALS AND HEATSINK ON PHOTOVOLTAIC PERFORMANCE

Ahmed Aljumaili[1], Yaser Alaiwi[2], Zainab Al-Khafaji[3,4*]

[1,2] *Department of Mechanical Engineering, Altinbas University, Istanbul 34217, Turkey*
[3] *Department of Civil Engineering, Faculty of Engineering and Built Environment, Universiti Kebangsaan Malaysia, 43600 UKM Bangi, Selangor, Malaysia*
[4] *Imam Ja'afar Al-Sadiq University, Baghdad, Iraq*

[1] https://orcid.org/0000-0003-0916-1807
[2] https://orcid.org/0009-0002-0829-5141
[3] *https://orcid.org/0000-0002-5450-7312*

Received 02/09/2023 ***Revised 09/01/2024*** ***Accepted 05/02/2024***

Abstract: This research aims to improve thermal performance and compare the performance of two common crystalline PV panel types (Mono and poly). Modules with a back-cooling system were designed and numerically analyzed with SolidWorks and ANSYS-Fluent-2021-R2 for the simulation under Baghdad weather at noon. The cooling system used consists of a phase-change material, paraffin wax (RT55), with a thickness of 5 cm and a heatsink with 33 fins with heights of 10, 20, and 30 mm and thicknesses of 2, 4, and 6 mm. to select the best height of the wax 1, 3, 5, 10, 20 cm examined. The result showed that for polycrystals, the panel temperature was reduced by 8.4°C using PCM and 11.9°C using PCM-fins. Also, output power was enhanced to 200.6 W by 10.2 W, and efficiency improved by 5%. Similarly, using PCM and PCM-fins lowered the temperature of the monocrystalline by 8.3 and 12.5°C, respectively. Therefore, the output power is enhanced to 202.4 W by 10.7 W and improves the electrical efficiency by 5.2%. The results of the study showed that mono had better performance than poly. This result is acceptable and is in good agreement with previous studies.

Keywords: *Cooling System; Heat dissipation; Mono-Polycrystalline; Paraffin wax; Photovoltaic modules*

1. Introduction

The utilization of alternative energy sources to fulfill the growing electricity and heating requirements is rising globally, especially in nations blessed with abundant renewable resources [1–4]. The increasing urgency for clean energy solutions has been driven by the detrimental impact of greenhouse gases on the environment, primarily caused by the ongoing reliance on fossil fuels to fulfill global energy needs [4–13]. Solar photovoltaic (PV) power is a highly prevalent globally widely adopted clean energy technology globally. It is one of the most commonly utilized and recognized clean energy solutions [14–16]. PV panel consists of solar cells that efficiently convert solar irradiance into a steady flow of electrical charges. The ongoing advancements in solar technologies, particularly in efficiency and cost-effectiveness, have resulted in a significant rise in its adoption [17,18]. While solar technology has gained

*Corresponding Author: *p123005@siswa.ukm.edu.my*

significant global adoption, it faces challenges. These include a reduction in efficiency as operating temperatures rise, relatively low energy conversion rates, and the accumulation of dust on module surfaces, which can hinder the technology from reaching its full operational potential [19,20]. An increase in the temperature of a PV panel can impact its operational parameters, leading to a decrease in the overall efficiency of the power plant [21]. According to research findings, it has been observed that for every 1°C rise in the surrounding temperature, there is a decrease in the performance efficiency of PV systems by approximately 0.4–0.5% [19]. Another factor highlighting the significance of effectively cooling PV panels is its positive impact on panel longevity. By mitigating the degradation rate, proper cooling measures contribute to extending the operational lifespan of the panels. Based on the findings by Royo et al. [22], it has been observed that the operational lifespan of PV systems can be extended significantly, from the typical 25-30 years to approximately 48 years, by implementing targeted cooling techniques.

Over the past decade, the utilization of solar energy has witnessed a significant surge in numerous countries, primarily driven by escalating fuel costs and the finite nature of traditional resources. Photovoltaics, as a solar energy technology, excels in efficiently converting solar radiation directly into electrical energy. The perpetual rise in energy demand has sparked a surge in enthusiasm towards energy efficiency and renewable energy technologies [23]. Building owners encounter a substantial predicament in reducing the expenditure associated with electricity bills, particularly in the case of hospital buildings that operate incessantly for 24 hours [24]. Simultaneously, this alternative energy source is perceived as a viable resolution to the utility costs in medical facilities due to its provision of reduced electricity tariffs alongside environmentally friendly power generation [24]. Moreover, the utilization of clean energy aligns with the worldwide dedication to mitigate carbon emissions and attain carbon neutrality. PV systems, in their essence, are meticulously engineered to harness the potential of solar energy as a viable substitute for the conventional power supply derived from the grid system. Nevertheless, PV panels exhibit the undesirable phenomenon of generating superfluous thermal energy while undergoing the power generation procedure. This surplus heat energy subsequently elevates the temperature of the PV cells, thereby causing a decrement in the overall efficiency of the installed system. Continuous exposure of PV panels to prolonged heating can potentially lead to structural damage [25].

Presently, many technologies are being suggested to enhance the efficiency of PV panels by extracting undesired heat utilizing suitable cooling methodologies and proficient thermal control techniques. The integration of both applications on PV modules yields a photovoltaic thermal system (PVT) that concurrently produces electrical power and captures excess thermal energy [26]. An adequate cooling methodology is imperative to uphold the surface temperature of the PV panel, thereby augmenting the overall efficiency of the PV system. In essence, PV cooling technology can be classified into three distinct categories: passive cooling, active cooling, and a hybrid approach that combines elements of both [27]. The utilization of commercially available cooling technologies in this context necessitates the provision of external power sources or the implementation of appropriate materials to

enhance the efficiency of PV cells. The optimization of solar energy harnessing from the PV system relies heavily on the utilization of efficient PV panels. A rapid decrease in solar panel efficiency may accelerate its disposal and create more landfills and associated environmental issues related to the fabrication of photovoltaic modules [28].

Phase change materials (PCMs) are chemical compounds with a substantial latent heat value, typically falling within the 100 - 280 kJ/kg range, contingent upon the material's inherent characteristics [29]. PCMs exhibit distinctive properties that enable them to store and regulate thermal energy, facilitating temperature stabilization effectively. These substances are commonly employed to extract surplus heat from PV installations owing to their inherent capacity to assimilate and retain substantial energy. PCMs exhibit distinctive properties that enable them to store thermal energy and facilitate temperature regulation effectively. The phase transformation process can alter the physical state of fluids and gases using condensation and evaporation, subsequently transitioning them into solid and liquid states through melting or freezing. As the temperature in the vicinity of the PCM increases to reach its melting point, the intermolecular bonds initiate an endothermic reaction, enabling the PCM to undergo energy absorption. The material undergoes a phase transition, transitioning from a solid state to a liquid state. As the temperature decreases to the freezing point of the PCM, the intermolecular bonds undergo regeneration, releasing heat to the surrounding environment [30,31].

The utilization of PCM strategically positioned at the rear of photovoltaic panels is elucidated, among other sources, in the scholarly article authored by Hamdan et al. [32]. A PCM was selected as the cooling substance due to its melting point proximity to the panels' standard test condition (STC) temperature. A PV system comprising two identical PV panels was analyzed. The PCM was strategically integrated onto the posterior surface of one panel. In contrast, the other panel remained in its conventional state, serving as a reference for comparative analysis. The experimental observations over 28 days exhibited a notable enhancement in power output by 2.6% when contrasted with panels not subjected to cooling measures.

Arıcı et al. [33] introduced a method for cooling PV systems using paraffin wax, an organic PCM characterized by its substantial latent heat capacity. The utilization of PCM is technically justified due to its ability to decrease the operational temperature of the PV panel by a maximum of 10.26°C, increasing electrical efficiency by up to 3.73%.

The current project aims to enhance the performance and output electrical power of two types of photovoltaic panels, monocrystalline and polycrystalline, by reducing the temperature of the solar cells, which are made of semiconductor materials such as silicon. Temperatures above 25°C negatively impact the efficiency of cells, reducing the panels' temperature importance [34]. It has been established that there is a decrease in efficiency of 0.4% for every degree above 25°C. The study will involve a comparative analysis of the performances of the two types of panels under challenging weather conditions, specifically in Baghdad City during the noon period, where temperatures are known to be high. The research will employ a cooling system that integrates PCM and a heatsink and uses simulation software, Ansys Fluent, to predict the thermal behavior and performance of the panels.

2. Theoretical Analysis

The ability of solar panels to produce energy is influenced by several factors, two of the most crucial elements in this simulation study: solar radiation and panel temperature. Variations in panel radiation and temperature variations accompany a solar panel's voltage, power, and electrical efficiency. To display the generation current, use the following formula:

$$I = I_{LG} - I_{OS} exp\left(\frac{q}{nkT_P}(V + IR_f)\right) - 1\Big] - \frac{V+IR_S}{R_{SH}} \quad (1)$$

Where:

The charge of an electron is a well-known value, designated as q, and it is equal to 1.602*10-19. Several factors can have an impact on the performance of a PV panel, including the air temperature (TP), the resistance within the panel's electrical circuit (Rs and R-SH), the energy of the silicon band gap (EGO), and the size of the panel (A). Coulomb's constant (n) is a factor that determines the efficiency of the diode within the panel, and it can range from 1 (for an ideal diode) to 2 (for practical diodes) [35].

Fig. 1 shows the equivalent electrical circuit of a PV cell, where the current is represented at the output terminals. This current equals the light-generated current. The internal resistance of the PV cell consists of the series resistance, Rs, and the shunt resistance, Rsh. For an ideal PV cell, Rs = 0 means there is no series loss, and Rsh = ∞means no leakage to the ground. The short circuit current, ISC, is the highest current a PV cell can produce when the cell is shorted. Meanwhile, the open circuit voltage, VOC, is the highest voltage at zero current flow when the two terminals of the PV cell are disconnected [36].

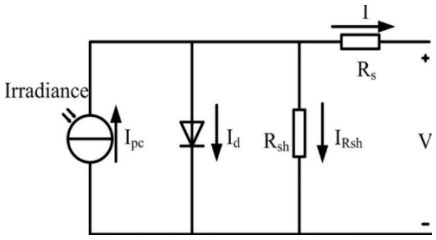

Figure 1. Electrical equivalent circuit of a photovoltaic module [37].

In Fig. 2, point A, also known as the max-out PowerPoint, is the functional point (P-max) at which the power is maximized [38]:

$$P_{max} = I_{max}V_{max} \quad (2)$$

$$P_{max} = I_{sc}V_{oc}FF \quad (3)$$

Whereas:

$$FF = \frac{P_{max}}{I_{sc}V_{oc}} \quad (4)$$

This formula can be employed to calculate the electrical efficiency of the module at (p max)

$$\eta = \frac{P_{mp}}{GA} \times 100 = \frac{I_{mp}V_{mp}}{GA} \times 100 \quad (5)$$

Where A is an area of the photovoltaic panel [39].

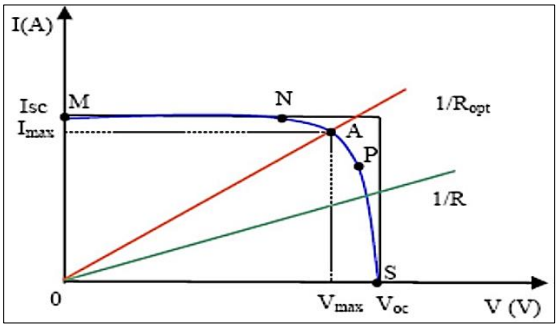

Figure 2. A typical current-voltage curve for solar cells.

The following equation can be used in the Ansys program to compute the electrical efficiency of solar cells [40].

$$\eta_{cell} = \eta_{ref}[1 - \beta(T_{cell} - T_{ref})] \quad (6)$$

Where reference panel efficiency is given by η ref=15% and β_{ref}, and the temperature coefficient is equal to 25°C, 0.3%, and 0.4 %, respectively. G indicates the standard solar irradiation: G = 1000 W/m2. For most PV cells,

such values are supplied by the manufacturer's product page [41].

A PV module's electrical power production can be evaluated as [42].

$$P_{out} = \eta_{ref}\left[1 - \beta_{ref}\left(T_{PV} - T_{ref}\right)\right]AG_{module} \quad (7)$$

3. System Geometry

The solar panels, the phase-changing material container, and the heat sink fins were designed in the Ansys Design Modular. It was considered that the design process was conducted in 2 steps. The 1st step represents the design of the heat sink in a flat and is linked with the solar panel. The complete design geometry of the present system is indicated in Fig. 3 and Table 1. Certainly, the change includes the height of the phase-changing material to see the effect of height on the results, where five dimensions were taken from the height of the phase-changing material: 1mm, 3mm, 5mm, 10mm, 20mm, represented by the dimension (H). The thickness of the aluminum is considered constant as 3mm, represented as (δ).

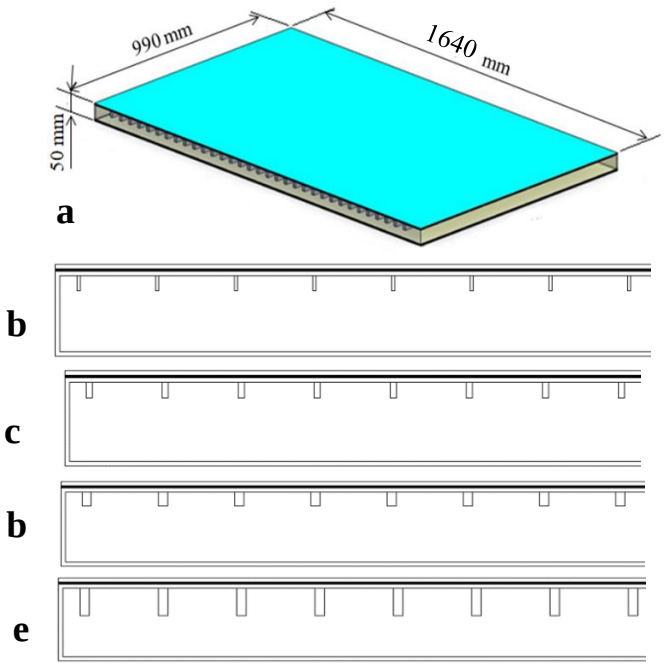

Figure 3. a) Overall design) (h=10, t=2) mm, c) (h=10, t=4) mm, d) (h=10, t=6) mm, e) (h=20, t=6) mm, f) (h=30, t=6) mm.

Table 1. Cases dimensions description

Case ID	Fins description	
	Height (h) mm	Thickness (t) mm
Case 1	10	2
Case 2	10	4
Case 3	10	6
Case 4	20	6
Case 5	30	6

3.1. Mesh Generation

About seven tries have been conducted to choose the optimum mesh, shown in Figs. 4 and 5. After changing the cell count from 240,000 to 270,000, the temperature and power have not significantly changed, hence the 2. Hence, cell mesh count was chosen for all the cases.

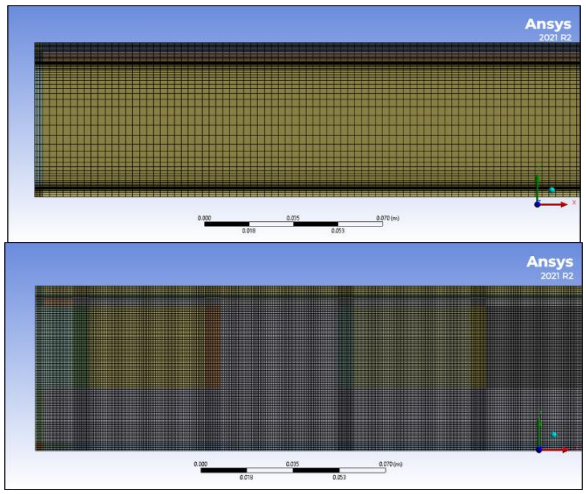

Figure 4. Structured mesh for the PV-PCM only and the Fin Case 5.

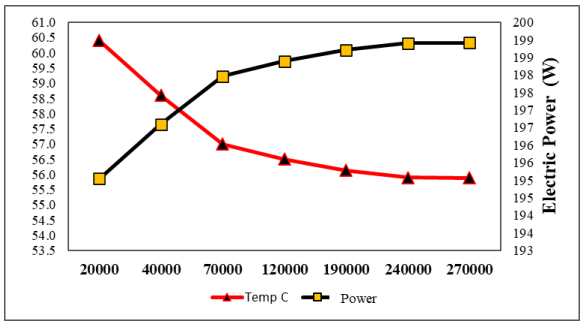

Figure 5. GIT for the PV-PCM-only case.

3.2. Boundary Conditions of the System

The maximum heat flux falling on the solar panel from 11 to 12 PM on a particular day in August is 955 W/m2, according to the meteorological data for that day. For the city of Al-Jadiriyah, Baghdad, Iraq, with a latitude and longitude line of (44.38, 33.28). The system consists of a solid PCM maintained at a temp, Tin, below the melting point, Tm, of the utilized PCMs at time t = 0. No-slip boundary constraints are also taken into consideration at the solid-fluid interfaces. Furthermore, all existing solid-solid interactions have a boundary condition that is thermally related.

Using Eq. (8), the heat from the solar radiation absorbed by each layer in the photovoltaic cells is computed and added to the heat transfer equation as an internal heat generation.

$$q_i = \frac{(1-\eta_{sc})\, G\, \alpha_i \tau_j\, A_i}{V_i} \qquad (8)$$

Where qi is the layer 1 internal heat production as a percentage of its volume; η stands for the silicon layer's electrical efficiency in solar cells; all other layers have a value of 0. G stands for solar radiation, whereas α, V, and A represent the absorptivity, volume, and area of layer 1, respectively. The layer above has a Transmissivity of τ. I [43].

In addition, as shown in Fig. 6, adiabatic boundary conditions are applied on the upper and lower ends of the PV–PCM system. The thermal boundary situation of the PV cell's top surface is a combination of convection and radiation dissipation. Accurate specifications should be made for the external radiation heat, surface external emissivity, air temperature, and heat transfer convection heat transfer coefficient PCM system and the PV system without the PCM; the external back boundary is prone to convective heat loss as well as convection and radiation losses. (h-conv) For the front side, it was 10, and half of this value was utilized for the rear side when simulating the worst-case scenario. The wind speed was 1 m/s. Table 2 provides a detailed expression of the applicable boundary conditions for the front and exterior back surfaces.

Table 2. Boundary conditions of the present study

Surface	Boundary condition
To the front of the Pv panel [43]:	$-k_g \frac{\partial T}{\partial x} = h_{\text{conv,g-amb}}\left(T_{amb} - T_g\right) + h_{rad,g-sky}\left(T_{sky} - T_g\right)$
On the PV-PCM system's back's outer surface:	$-k_{al} \frac{\partial T}{\partial x} = h_{\text{conv},al-amb}\left(T_{amb} - T_{al}\right)$
On the PV cell's outer rear surface without the PCM:	$-k_T \frac{\partial T}{\partial x} = h_{\text{conv},T-amb}\left(T_{amb} - T_T\right) + h_{rad,T-sky}\left(T_{sky} - T_T\right)$
h from glass to environment [44]:	$\boldsymbol{h_{\text{conv, g-amb}} = 5.7 + 3.8V_w}$
Radiative σ from glass to the sky [45]: And from Tedlar to sky:	$\boldsymbol{h_{rad,g-sky} = \sigma \varepsilon_g \frac{\left(T_g^4 - T_{sky}^4\right)}{\left(T_g - T_{sky}\right)}}$

The Sky Temperature [45]	$T_{sky} = 0.0522T_{amb}^{1.5}$

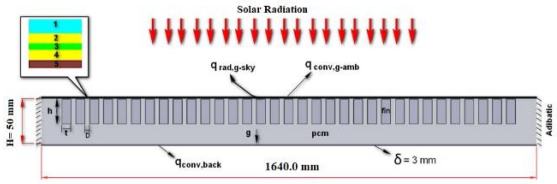

Figure 6. PV-PCM-Fin system schematic.

3.3. Solar models

The polycrystalline and monocrystalline solar panels were carefully selected from the Chinese business Ningbo Rarlon Photovoltaic Technology Co. and the Max Power Company to assist in the comparison procedure. The dimensions of the chosen panel are 1640 x 990 x 40 mm, and the cell size is 156 x 156 mm. The NO of cells is 60 as s60 cells, Fig. 7, Table 3 listed the solar panel electrical properties.

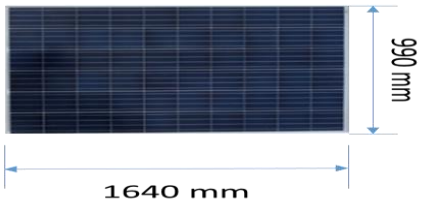

Figure 7. Poly solar panels.

Table 3. Electrical characteristics of solar panels

Type	Polycrystalline	monocrystalline
Pmax	250 W	250 W
Vmpp	30.45V	30.72V
Impp	8.21A	8.138A
(Voc)	36.54V	36.91V
(Isc)	9.44A	9.031A
efficiency %	15.3 %	15 .39 %
dimension(L*W)	1640*992 mm	1640*992 mm
B	-0.45 %/°C	-0.35 %/°C

3.3.1. Properties of the PV module layers (poly)

Commercial solar panels are made up of several layers, including a transparent top layer of glass and a transparent EVE layer to protect the cells from weather conditions and high temperatures, as well as a lower packing layer of EVE and an aluminum back metal plate to protect the plate from the wind and the cell's edge [46]. Tables 4 and 5 listed the poly and monocrystalline layer specifications, respectively.

Table 4. Specification of Poly layers [47]

Components	ρ kg/m3	t (m)	Cp J/kg K	k W/m.K	ε	α	τ
Glass	3000	0.003	500	2	0.9	0.04	0.92
Si solar cell	2330	0.0002	677	148	-	0.9	-
EVA layer	960	0.0005	2090	0.35	-	0.08	0.90
Tedlar TPT	1200	0.0003	1250	0.2	0.9	-	-

3.3.2. Properties of the PV module layers (mono)

Table 5. Specification of monocrystalline layers [48].

Components	ρ kg/m3	t (mm)	Cp J/kg K	k W/m.K
Glass	2300	3	0.50	1
Si cell layer	2330	0.35	0.757	168
EVA layer	960	0.50	2.09	0.35
Tedlar TPT	1500	0.20	1.20	0.20

Furthermore, the transitivity of the glass cover for monocrystalline is τg = 0.95, the solar cell

absorptivity is αc 0.85, and finally, the absorptivity of TPT is αT = 0.5 [49].

3.4. Materials

3.4.1. Fins of the heat sink

A heatsink dissipates the heat solar radiation generates into the environment. The heat sink's thermal conductivity plays a role in its ability to dissipate heat, and the amount of heat that needs to be dissipated is influenced by the contact area between the heatsink and the environment. Increasing the number of fins on the heatsink can increase the contact area and improve heat dissipation [50]. The material used for the fins is aluminum due to its frequent use in such works and the ease of its formation. Note its properties as in Table 6 [47].

Table 6. Thermophysical Properties of Aluminum [47].

Thermophysical properties	Aluminum
ρ kg/m^2	2675
K w/k.m^2	211
CP kJ/kg.k	0.093

3.4.2. PCM

One of the most popular PCMs is paraffin wax, which has several beneficial characteristics. The melting temperature of the paraffin wax utilized in this project is around 5°C. It was provided by RUBITHERM and is known by the trade name RT55, as demonstrated in Fig. 6 and Table 7 shows the paraffin wax RT55 thermophysical properties.

Table 7. Thermophysical properties of paraffin wax RT55 [51].

Thermophysical properties	RT55
Melting point °C	51-57
Cp (kJ/kg)	170
K (w/k.m^2)	0.2
Specific heat capacity (kJ/kg.k)	2
ρ - Solid kg /m^{-3}	880
ρ - Liquid kg /m^{-3}	770
Volume expansion %	14

4. Result And Discussion

4.1 Validation

To validate the achieved were compared to experimental data or analytical solutions, which proved to validate a simulation in ANSYS Fluent ensures the simulation's correctness and dependability, which is carried out to ensure that the simulation results appropriately reflect the system's behavior under simulation. The validation process may be carried out with simulation findings to experimental data through charting or statistical analysis, the validated simulation setup, and the numerical techniques utilized; the simulation results may also be contrasted with analytical answers; the validation procedure enhances the reliability and accuracy of the simulation findings.

4.1.1 Model Validation

The ANSYS Fluent software was utilized to model the performance of a solar model with and without a cooling method. The cooling system consisted of a phase-changing material and an aluminum frame behind the panel. The simulation was run using the same boundary conditions, temperatures, and material properties as in a reference article (Mohamed Emam et al.,[47]) to test the accuracy and predict the melting of the phase-changing material and the surface temperature of the model.

4.1.2 Validation of the uncooled PV concentrator model

The expected results were compared with the experimental results of the reference article, and through simulation, a solar concentration of CR = 5, 10, and 20 was used, which is equivalent to 50,000, 10,000, and 20,000 w/m2 of incident solar irradiation, and the temperature was compared with the time. As the concentration

intensity increases, the heat of the plate's front surface rises over time, and the simulation's boundary conditions are 20°C atmospheric temperature and 1 m/s wind velocity with a period length of 50 minutes. As shown in Fig. 8, the predicted findings were substantially equal to the experimental results of the study publication [47], and the most significant error rate was exceptionally low.

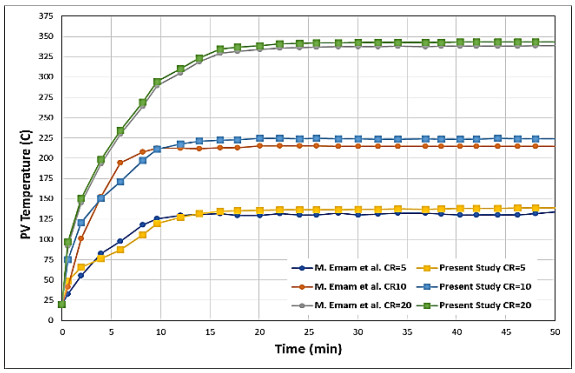

Figure 8. Validation for PV only without PCM with a reference article.

4.1.3 *Validation of the PV concentrator model with PCM*

The validity of the research's numerical results has validated the expected result for the temperature distribution and solubility of a phase-change material with time has been valium material is n-octadecane paraffin, which has a melting point of 28°C and thermal conductivity coefficients of 0.358 and 0.148 (W/m°C) for the solid and liquid situations, respectively. The simulation time was only 40 minutes, the concentrated solar radiation was 10, the ambient temperature was 20°C, and the wind speed was 1m/s. The results showed the melting of the (PCM) and the temperature of the panel in a manner very similar to the numerical results of the research. The error rates did not exceed 5%, as shown in Figs. 9 and 10, which display the predicted validation, solidification, and melting (PV-PCM).

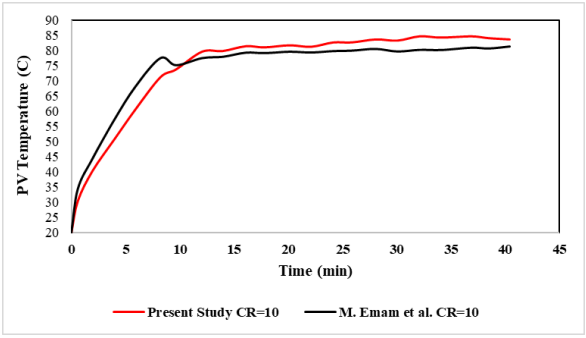

Figure 9. Validation for PV-PCM with Emam et al., [52].

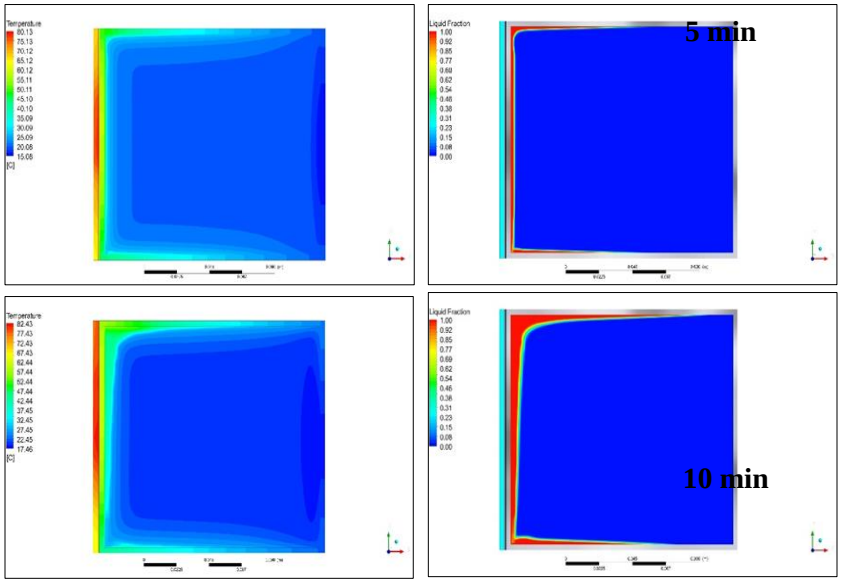

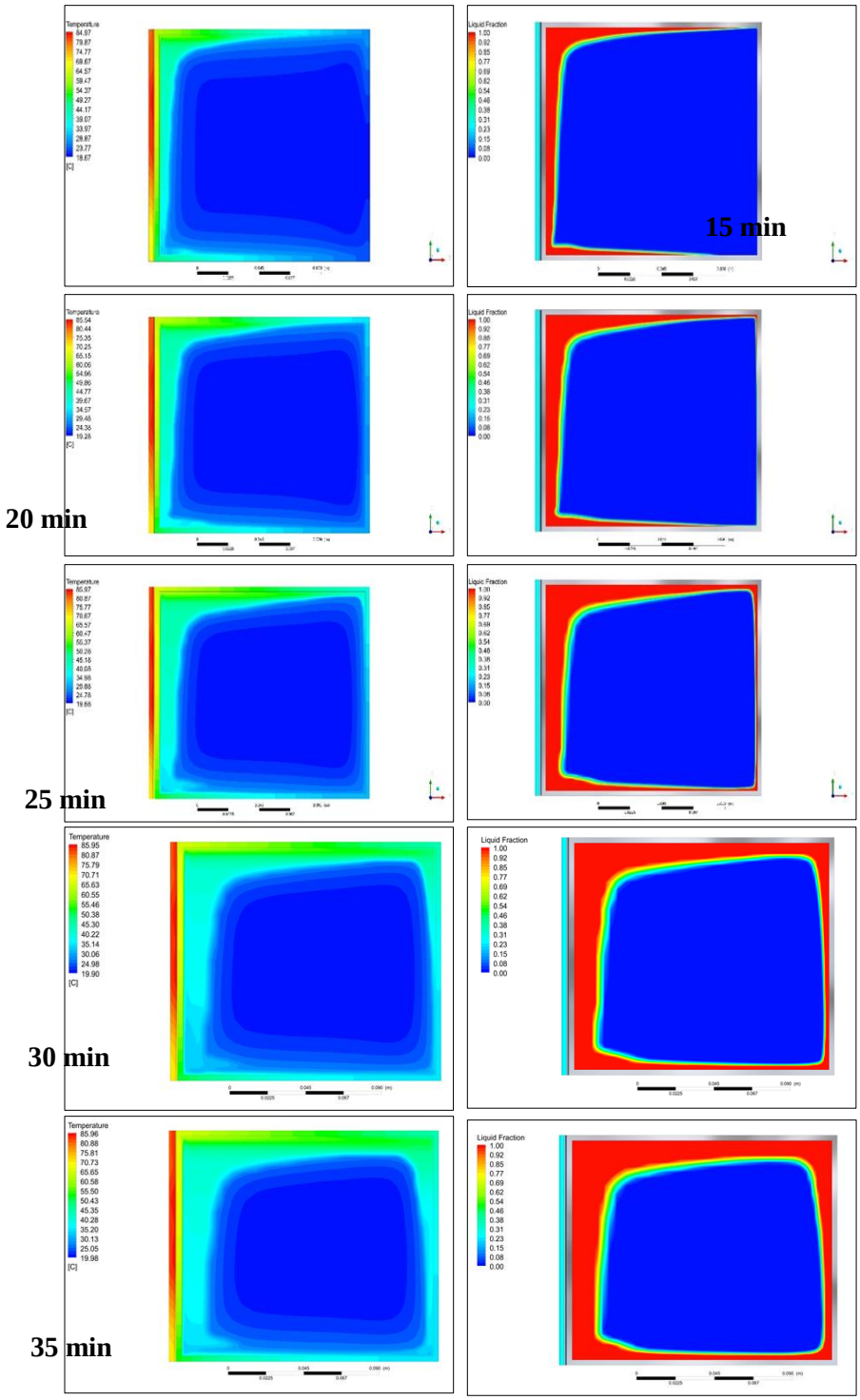
15 min
20 min
25 min
30 min
35 min

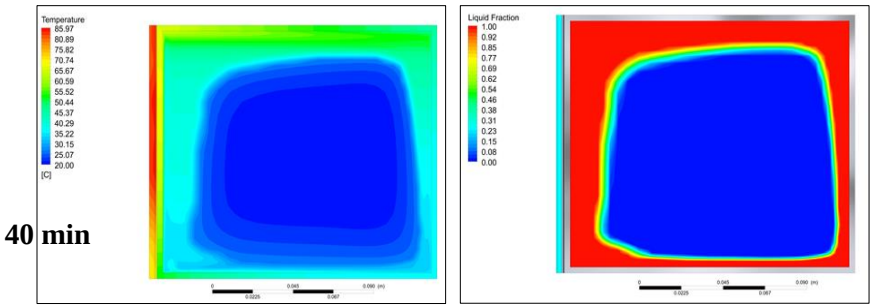

Figure 10. The CPV-PCM1 predicted isotherms and analyses the liquid-solid interaction, where red represented the liquid and blue represented the solid. CR= 5, 10, 15, 20, 25, 30, 35 and 40 min

4.2 Effect of wax thickness on cell performance

To determine the optimal wax thickness, examine various wax layer heights for 3600 seconds and obtain the following results, as shown in Fig. 11.

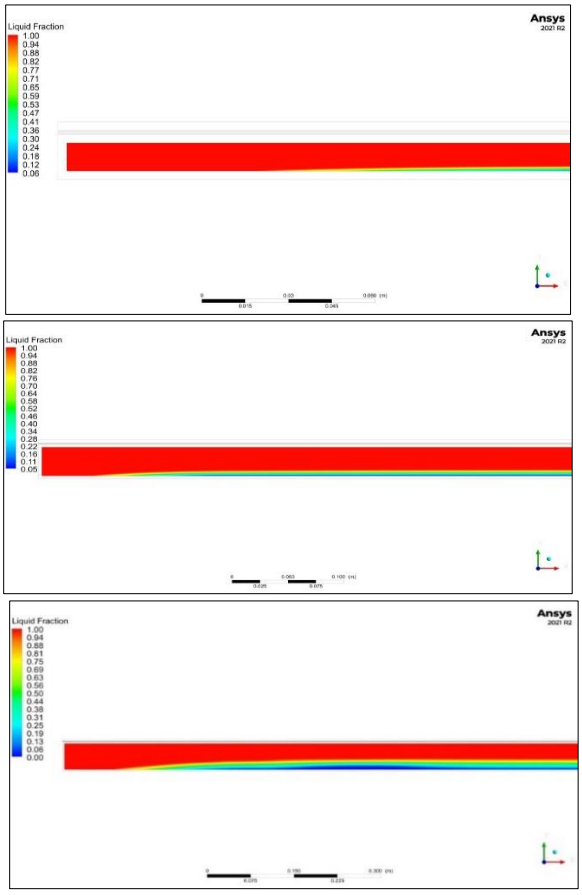

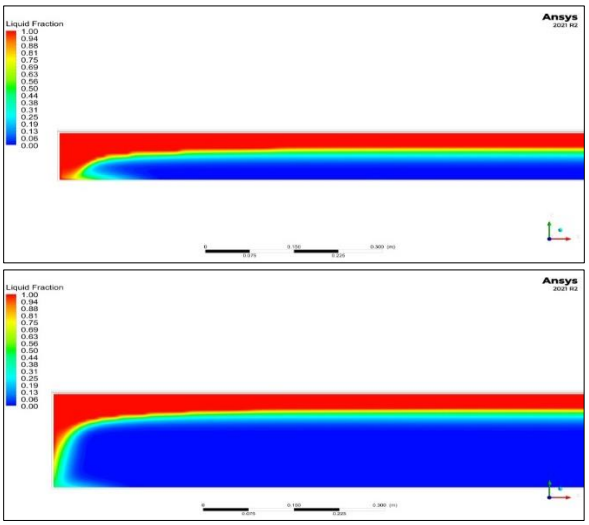

Figure 11. Liquid fraction wax layers of 1, 3, 5, 10, and 20 cm thickness for 3600 seconds.

Fig. 12, which depicts the liquid fraction interfaces between PCM solid-liquid phases, demonstrates how different locations in the PCM layer behave similarly when phases change. A tiny piece of the PCM layer begins to melt after 10 minutes, whereas locations further from the interior surface take around 20 minutes to reach the liquid state. The quantity of the molten layer increases after 30 minutes. For thicknesses of 1 and 3 cm, the melting process is completed in 60 minutes; however, for thicknesses of 5 and 20, a greater portion of the material is still solid. The tiny thicknesses of 1 and 3 cm are the cause of this. The heated liquid

may be transported to the final location using only a convection current. Due to the hot currents' inability to reach certain solid regions due to inadequate buoyancy force, an unmolten portion of the wax may persist as the wax thickness grows. As a result, these layers take longer to melt. Most of the PMC layer is already in the molten phase after 60 minutes, and no heat discharge occurs. Red denotes a liquid zone, followed by blue, a solid region, and ultimately green, which denotes the start of a phase shift.

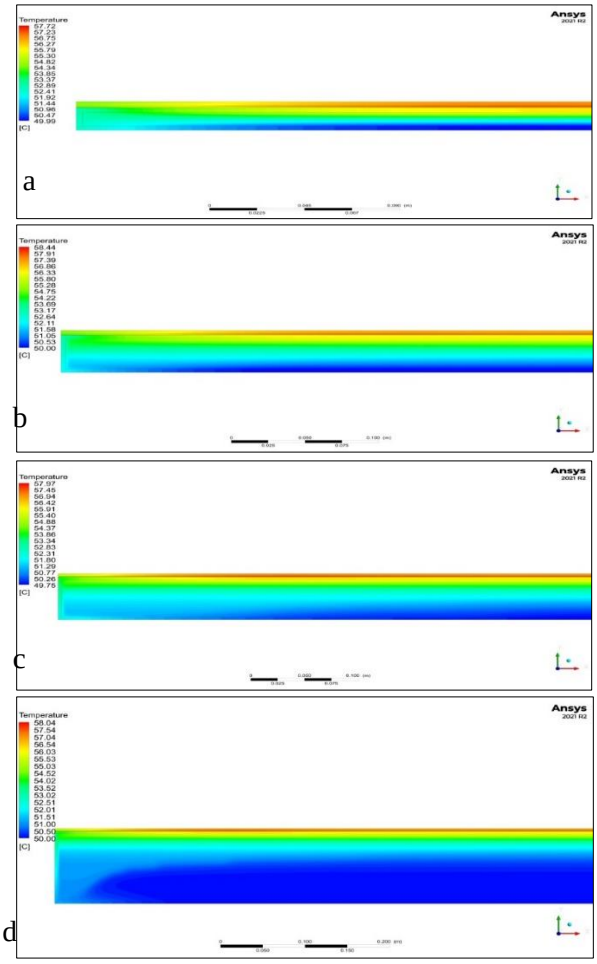

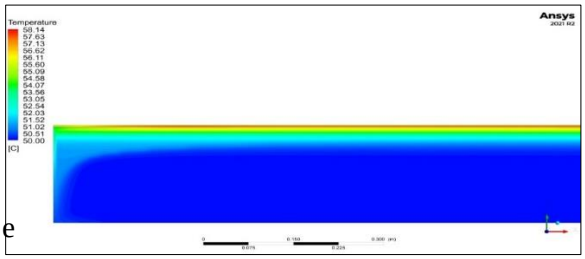

Figure 12. Temperature contour to wax layers of 1, 3, 5, 10, and 20 cm thickness for 3600 seconds.

The temperature contours of a PV-PCM cell during the phase change process are indicated in Fig. 13. The contours are divided into two regions: a maximum hot region (represented by red) and a color cool region (represented by blue). At 10colourtes, the maximum temperature of the wax for thicknesses of 1, 3, 5, 10, and 20 cm was recorded as 52.8, 52.9, 52.82, 52.83, and 52.85°C, respectively. The melting process did not commence as the temperatures were below the melting point of the wax. The temperatures gradually increased due to the wax's increased convection heat transfer and thermal conductivity. At 30 minutes, the maximum temperatures recorded were 55.04, 55.39, 55.1, 55.14, and 55.2^{o}C, respectively. As the convection continued, the temperature continued to rise. By 60 minutes, the melting of the wax was complete, and a thermal equilibrium stage began for thicknesses between 1 and 3 cm. The temperatures recorded at this stage were 57.01, 57.7, 57.37, 57.43, and 57.53°C, respectively.

Fig. 13 PV only without using PCM recorded a maximum value of (65.75), while PV with PCM in 1 cm recorded a minimum value of (57.08). After studying the influence of the thickness, we selected a 5 cm thickness as the optimal thickness for improving the cooling of the board and its performance by adding fins of various sizes and dimensions.

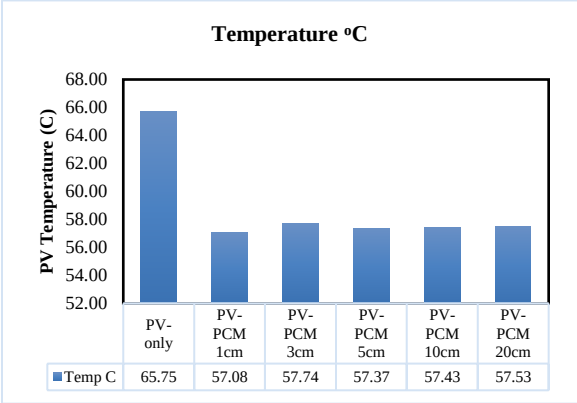

Fig. 13. PV temperature with PCM layers of 1, 3, 5, 10, and 20 cm thickness after 3600 seconds.

4.3 Polycrystalline PV module

Multi-crystalline or polycrystalline PV panels are solar panels composed of several tiny crystal structures rather than a single, larger crystal structure. To create the monochrome into a square mold, chop it into smaller, individual wafers.

Fig. 14 shows the temperature distribution through the PV layers (glass to tedlar) when exposed to incident irradiation conditions equal to 955 w/m2, a wind velocity of 1 m/s, and an environment temperature of 50.1°C for 3600 seconds. Because of the silicon cell's high transmissivity and high absorption of sunlight, the cell temperature increased, reaching around 65.85°C inside the silicon layer; thus, the heat inside the cell increased over time, leading to an increase in heat but a lower level in Eva and Tedlar due to heat transfer to the environment. The red color shows the high temperature of the silicone layer, and the light blue color indicates the temperature of both the glass and the Tadler. The rate of rise in the panel's temperature fluctuated between 64 and 65.8°C. Therefore, it became necessary to cool the panels.

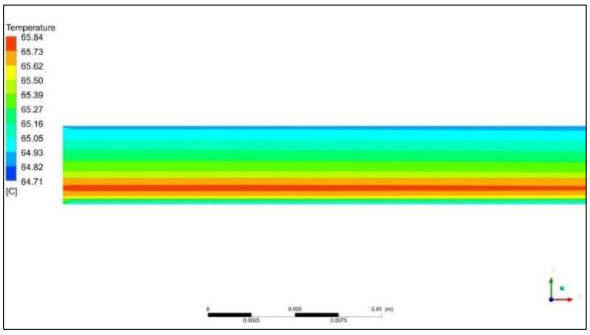

Figure 14. Temperature distribution of the PV cell only.

Fig. 15 illustrates the thermal transfer process in a layer of PCM used in a back-cooling device for a solar cell. The heat is transferred from the surface of the silicon cell to the PCM container through a convective heat transfer process. As the temperature of the PCM increases, it undergoes a phase change, transitioning from a solid to a liquid state.

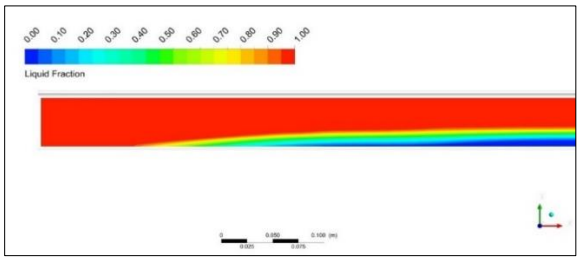

Figure 15. Liquid fraction distribution PV-PCM.

Fig. 16 shows temperature dispersion contours for PV-PCMF. It was found that the addition of aluminum fins with varying thicknesses of 2, 4, 6, and heights of 10, 20, and 30 mm in combination with a layer of PCM led to a significant decrease in the surface temperature of the panel. Specifically, the cell temperature dropped from 65.8°C in the PV-only to 53.9°C in the PCM-F, optimum case 5, with a thickness of 6 mm and a height of 30 mm. This reduction is due to the high thermal conductivity of aluminum and the increased heat transfer surface area provided by the fins [53]. The aluminum fins allow for a more efficient transfer of heat from the cell to the PCM,

absorbing heat faster and delivering it to the PCM more effectively.

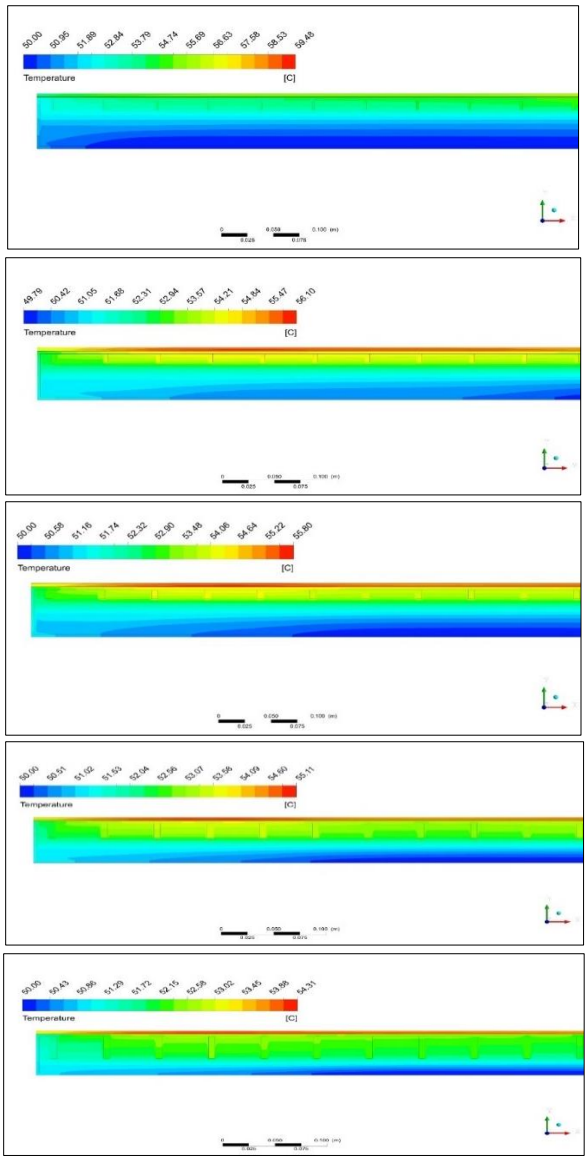

Figure 16. Temperature contour PV PCM- fins for all cases (1, 2, 3, 4, and 5).

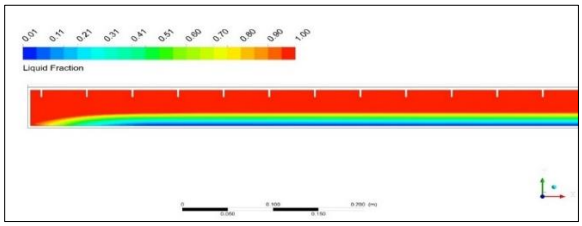

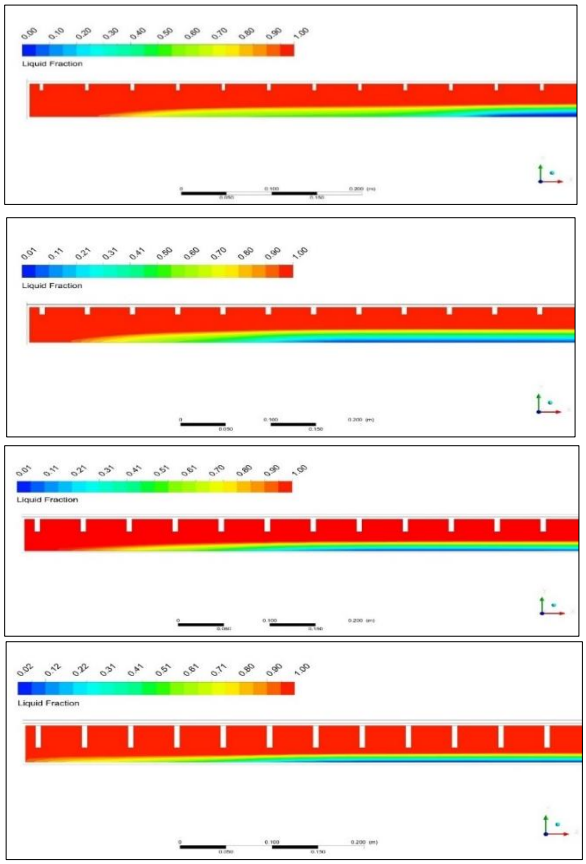

Figure 17. Liquid fraction PV PCM - fins cases 1, 2, 3, 4, and 5.

4.4 Monocrystalline PV module

Monocrystalline solar cells, made from thin silicon wafers, are the oldest and most popular type of solar cell technology. They have the highest efficiency, reaching up to 26%, which means that they produce more electricity per panel unit area than other solar photovoltaic PV technologies [54].

Fig. 18 depicts the temperature distribution contours for a monocrystalline PV-PCMF (Photovoltaic-Phase Change Material Fin). It can be observed that by incorporating fins into the PCM, the temperature within the PCM increases due to an enhancement in convection heat transfer, which leads to an increase in the overall thermal activity of the system over time due to the rise in surface area available for heat

transfer. The green layer, which represents the regions of high temperature within the PCM, is initially observed to be relatively thin. However, as the size of the fin changes, as depicted in Cases 4 and 5, the thickness of this high-temperature layer increases accordingly.

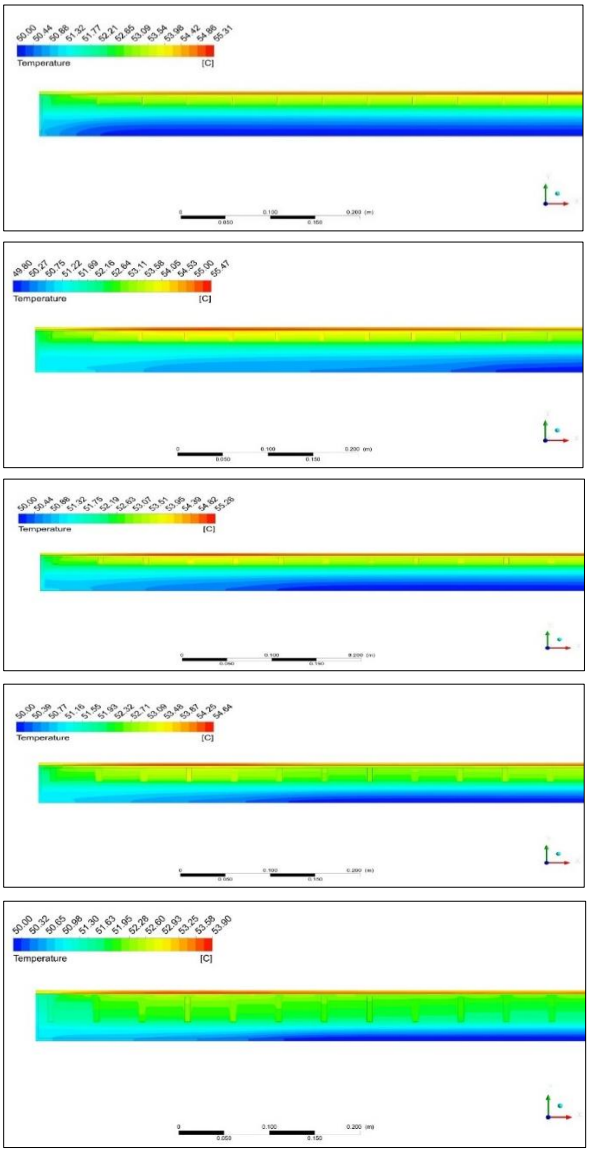

Figure 18. Temperature contour of the PV –PCM fins case 1, 2, 3, 4, and 5.

The liquid fraction Mono in Fig. 19, the liquid fraction PV-PCMF, and the phase change for various cases are depicted. In Case 1, it can be observed that the red color in Fig. 19 represents the thickness of the molten layer that forms at the contact points between the wall of the container and the fins. The molten layer begins to form due to the withdrawal of heat from the silicon cell to the wax through conduction, leading to hot currents and an increase in the thickness of the molten layer over time. Additionally, the yellow layer at the container's left edge indicates the beginning of the phase change due to the heating of the container wall through thermal conductivity.

In Cases 2 and 3, as the thickness of the fins changed, the amount of heat withdrawn enhanced, leading to a growth in the thickness of the molten layer due to the increase in hot currents flowing toward the solid phase. The increase in the yellow layer in these cases is due to the weak resistance of the solid layer to hot currents. In Case 4, an increase in the length of the fins results in enhanced heat transfer to the farthest solid area, leading to the fading of the solid area and its appearance as a thin layer. Over time, the wax will ultimately transition to the liquid phase.

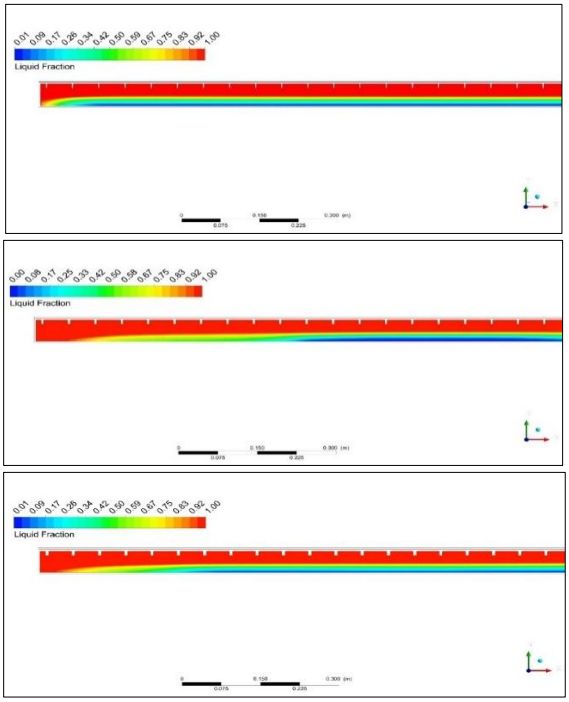

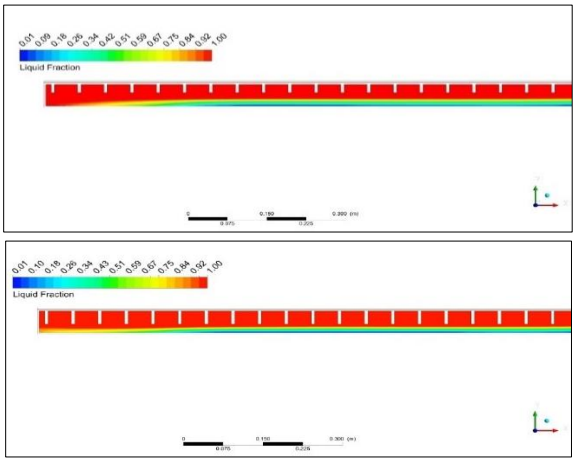

Figure 19. Liquid fraction PV–PCM fins cases (1, 2, 3, 4 and 5).

4.5 Comparison of poly-monocrystalline panels' performance

Fig. 20 compares the thermal performances of two types of panels, one monocrystalline and one polycrystalline, with and without cooling. The thermal performance of the monocrystalline panel is slightly better than that of the polycrystalline panel, which is because both the thermal performance coefficient and the thermal conductivity of the monocrystalline panel are better than those of the polycrystalline panel. The poly temperature was measured at 65.8^{o}C without cooling and mono at 64.3^{o}C; after applying PCMFs, the temperature notes were 53.9 and 51.8^{o}C, respectively. The monocrystalline panel is more effective at conducting heat and has a higher capacity for thermal performance, leading to better overall thermal performance.

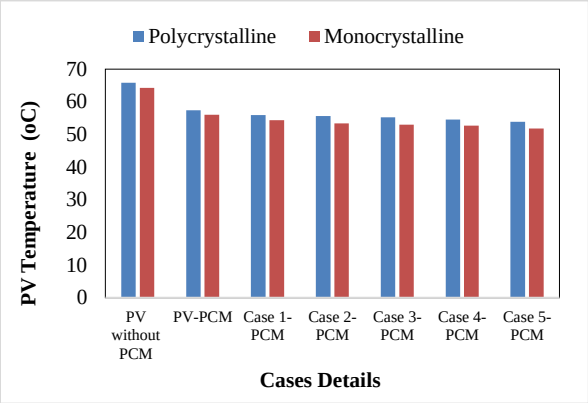

Figure 20. Thermal performance of mono-polycrystalline panels.

Fig. 21 compares the electrical performance of monocrystalline and polycrystalline models. The monocrystalline panel data performs electrically better with and without cooling than the polycrystalline panel because it recorded a slightly lower temperature, which leads to an enhancement in output power. After all, high temperatures can reduce electrical efficiency. Output power recorded for mono and poly with no cooling applied was 191.7 and 190.4 W, respectively, and with PCMF, it was 202.4 and 200.6 W, respectively, as shown in cases 1 and 5.

Fig. 22 compares the electrical efficiency between poly and monocrystalline photovoltaic cells, with and without cooling. The initial efficiency of the poly model was 12.93%, while the efficiency of the Monocrystalline model was 13.02%. Upon implementing PCMF, the electrical efficiency improved to 13.62% and 13.74% for the poly and monocrystalline models, respectively.

Observed that the monocrystalline model exhibited a slightly better electrical efficiency than the poly model, which can be attributed to the lower temperature of the poly model, leading to a marginal increase in output power

and efficiency. Thus, the monocrystalline model performs better in high-temperature conditions.

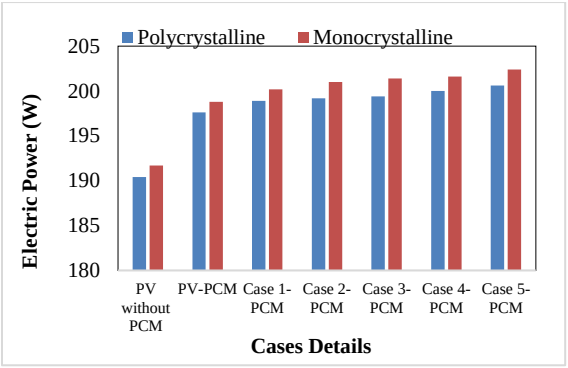

Figure 21. Electrical performance of monocrystalline and polycrystalline panels.

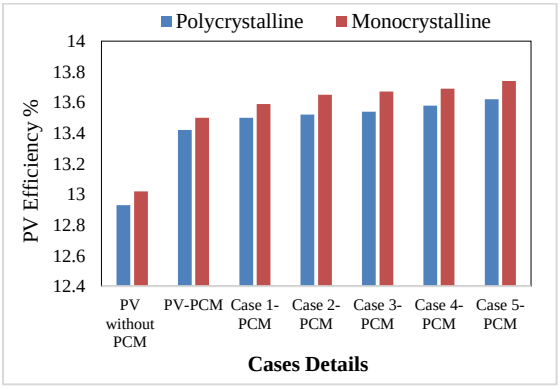

Figure 22. Monocrystalline and polycrystalline panel electrical efficiency

5. Conclusion

High panel temperatures, decrease its life. During max solar radiation of 955 w/m2 for an hour, the monocrystalline panel temperature was 1.5 degrees lower than the polycrystalline panel before applying wax and fins, which suggests that the monocrystalline panel is more resistant to temperature increases when exposed to high solar radiation levels. Also, applying paraffin wax without fins decreased the temperature of PV types by 12.77 and 12.91% for both polycrystalline and monocrystalline panels, respectively. Moreover, it increases the electrical power and PV efficiency by 3.7 and 3.78% for polycrystalline and monocrystalline panels, respectively. Increasing the fin thickness from (2-6) mm led to a decrease in the temperature of PV types by (15.4-17.57) % and (15.05-15.96) % for both monocrystalline and polycrystalline panels, respectively. Increasing the fin height from (10-30) mm led to a decrease in the temperature of PV types by (17.57-19.44) % and (15.966-18.09) % for both monocrystalline and polycrystalline panels, respectively. The monocrystalline panel is more effective at retaining a lower temperature when cooled using these methods. The monocrystalline model's output power was higher than the polycrystalline model by 1.3 watts before cooling and by 1.8 watts under the optimal cooling scenario. However, before cooling, the monocrystalline panel's electrical efficiency was 0.07% higher than that of the polycrystalline panel. After the best cooling strategy was applied, the difference in electrical efficiency between the two panels increased to 0.12%.

Nomenclature

Symbol	Description	Symbol	Description
PV	Solar photovoltaic	RT55	Paraffins Wax
PCMs	Phase change materials.	N	Diode Factor
ISC	Short Circuit Current	EGO	Band Cap Silicon
VOC	Voltage Open Current	FF	Performance Factor
Rs	Series Resistance	T cell	Cell Temperature
R-SH	Shunt Resistance	Tm	Ambient Temperature
GIT	Grid Independence	TPT	Back Sheet Tedlar

Author Contributions: All authors conducted the work equally.

Acknowledgments: The authors would like to reveal their appreciation and gratitude to the respected reviewers and editors for their constructive comments.

Conflicts of Interest: The authors declare no conflict of interest.

References

1. Hamza JE, Al-Kayiem HH, Lemma TA. Experimental investigation of the separation performance of oil/water mixture by compact conical axial hydrocyclone. Thermal Science and Engineering Progress 2020;17:100358. https://doi.org/10.1016/j.tsep.2019.100358
2. Almansory A, Al-Anbarri K. Security Constrained Optimal Power Flow Based On An Artificial Intelligence Technique. Journal of Engineering and Sustainable Development 2023;27:725–41. https://doi.org/10.31272/jeasd.27.6.5.
3. Hussein SAA, Nima MA. Numerical And Experimental Investigation Of Semicircular Solar Updraft Tower System Employing Porous Copper Metal Foam. Journal of Engineering and Sustainable Development 2023;27:596–614. https://doi.org/10.31272/jeasd.27.5.4.
4. Radhi SS, Al-khafaji ZS, Falah MW. Sustainable heating system by infrared radiators 2022;4:42–52. https://doi.org/10.37868/hsd.v4i1.82.
5. Agyekum EB, Velkin VI. Optimization and techno-economic assessment of concentrated solar power (CSP) in South-Western Africa: A case study on Ghana. Sustainable Energy Technologies and Assessments 2020;40:100763. https://doi.org/10.1016/j.seta.2020.100763.
6. Agyekum EB, Amjad F, Mohsin M, Ansah MNS. A bird's eye view of Ghana's renewable energy sector environment: a Multi-Criteria Decision-Making approach. Utilities Policy 2021;70:101219. https://doi.org/10.1016/j.jup.2021.101219.
7. Adebayo TS, Agboola MO, Rjoub H, Adeshola I, Agyekum EB, Kumar NM. Linking economic growth, urbanization, and environmental degradation in China: what is the role of hydroelectricity consumption? International Journal of Environmental Research and Public Health 2021;18:6975. https://doi.org/10.3390/ijerph18136975.
8. Al-Khafaji ZS, Al-Naely HK, Al-Najar AE. A review applying industrial waste materials in stabilisation of soft soil. Electronic Journal of Structural Engineering 2018;18:16–23. https://doi.org/10.56748/ejse.182602.
9. Hussain AJ, Al-Khafaji ZS. Reduction of environmental pollution and improving the (Mechanical, physical and chemical characteristics) of contaminated clay soil by using of recycled oil. Journal of Advanced Research in Dynamical and Control Systems 2020;12:1276–86. https://doi.org/10.5373/JARDCS/V12SP4/20201604.
10. Dr. Abdullah Jabar Hussain AZSA-K. The Fields of Applying the Recycled and Used Oils by the Internal Combustion Engines for Purposes of Protecting the Environment against Pollutions. Journal of Advanced Research in Dynamical and Control

Systems 2020;12:666–70. https://doi.org/10.5373/JARDCS/V12SP1/20201119.
11. Marshdi QSR, Hussien SA, Mareai BM, Al-Khafaji ZS, Shubbar AA. Applying of No-fines concretes as a porous concrete in different construction application. Periodicals of Engineering and Natural Sciences 2021;9:999–1012. https://doi.org/10.21533/pen.v9i4.2476.
12. Sattar S, Alaiwi Y, Radhi NS, Al-khafaji Z. Numerical Simulation for Effect of Composite Coating (TiO2 + SiO2) Thickness on Steam Turbine Blades Thermal and Stress Distribution. Academic Journal Of Manufacturing Engineering 2023;21. https://ajme.ro/current_issue.php
13. Hamza SA, Radhi NS. Composite Coating Using (Hap-Nano Silver) By Macro Arc Oxidation Procedures Was Used To Study the in-Vivo Properties of Titanium Substrate. Academic Journal of Manufacturing Engineering 2023;21:65–71. https://ajme.ro/content.php?vol=21&year=2023&issue=1&offset=0
14. Homadi A, Hall T, Whitman L. Study a novel hybrid system for cooling solar panels and generate power. Applied Thermal Engineering 2020;179:115503. https://doi.org/10.1016/j.applthermaleng.2020.115503.
15. Alwan NT, Shcheklein SE, Ali OM. Experimental investigation of modified solar still integrated with solar collector. Case Studies in Thermal Engineering 2020;19:100614. https://doi.org/10.1016/j.csite.2020.100614.
16. Alwan NT, Shcheklein SE, Ali OM. Experimental analysis of thermal performance for flat plate solar water collector in the climate conditions of Yekaterinburg, Russia. Materials Today: Proceedings 2021;42:2076–83. https://doi.org/10.1016/j.matpr.2020.12.263
17. Ahmad FF, Ghenai C, Hamid AK, Rejeb O, Bettayeb M. Performance enhancement and infra-red (IR) thermography of solar photovoltaic panel using back cooling from the waste air of building centralized air conditioning system. Case Studies in Thermal Engineering 2021;24:100840. https://doi.org/10.1016/j.csite.2021.100840.
18. Agbo EP, Edet CO, Magu TO, Njok AO, Ekpo CM, Louis H. Solar energy: A panacea for the electricity generation crisis in Nigeria. Heliyon 2021;7. https://doi.org/10.1016/j.heliyon.2021.e07016.
19. Sudhakar P, Santosh R, Asthalakshmi B, Kumaresan G, Velraj R. Performance augmentation of solar photovoltaic panel through PCM integrated natural water circulation cooling technique. Renewable Energy 2021;172:1433–48. https://doi.org/10.1016/j.renene.2020.11.138.
20. Karam EH, Mohammed YA, Kadhim NN. Controlling water level by using modified model free adaptive controller. Journal of Engineering and Sustainable Development (JEASD) 2023;27. https://doi.org/10.31272/jeasd.27.3.7.
21. Sudhakar P, Kumaresan G, Velraj R. Experimental analysis of solar photovoltaic unit integrated with free cool thermal energy storage system. Solar Energy 2017;158:837–44. https://doi.org/10.1016/j.solener.2017.10.043.
22. Royo P, Ferreira VJ, López-Sabirón AM,

Ferreira G. Hybrid diagnosis to characterise the energy and environmental enhancement of photovoltaic modules using smart materials. Energy 2016;101:174–89. https://doi.org/10.1016/j.energy.2016.01.101.

23. Shubbar A, Nasr M, Falah M, Al-Khafaji Z. Towards net zero carbon economy: Improving the sustainability of existing industrial infrastructures in the UK. Energies 2021;14:5896. https://doi.org/10.3390/en14185896.
24. Rahman NMA, Haw LC, Fazlizan A. A literature review of naturally ventilated public hospital wards in tropical climate countries for thermal comfort and energy saving improvements. Energies 2021;14:435. https://doi.org/10.3390/en14020435.
25. Suresh AK, Khurana S, Nandan G, Dwivedi G, Kumar S. Role on nanofluids in cooling solar photovoltaic cell to enhance overall efficiency. Materials Today: Proceedings 2018;5:20614–20. https://doi.org/10.1016/j.matpr.2018.06.442
26. Ghadiri M, Sardarabadi M, Pasandideh-fard M, Moghadam AJ. Experimental investigation of a PVT system performance using nano ferrofluids. Energy Conversion and Management 2015;103:468–76. https://doi.org/10.1016/j.enconman.2015.06.077.
27. Sato D, Yamada N. Review of photovoltaic module cooling methods and performance evaluation of the radiative cooling method. Renewable and Sustainable Energy Reviews 2019;104:151–66. https://doi.org/10.1016/j.rser.2018.12.051.
28. Hamzat AK, Sahin AZ, Omisanya MI, Alhems LM. Advances in PV and PVT cooling technologies: A review. Sustainable Energy Technologies and Assessments 2021;47:101360. https://doi.org/10.1016/j.seta.2021.101360.
29. Trahan J. A technical and economic comparative analysis of sensible and latent heat packed bed storage systems for concentrating solar thermal power plants. University of South Florida; 2015.
30. Al-khafaji ZS, Radhi NS, Mohson SA. Preparation and modelling of composite materials (polyester-alumina) as implant in human body. International Journal of Mechanical Engineering and Technology 2018;9.
31. Al-Khafaji ZS, Radhi SS, Mahdi MM, Radhi NS, Mareai BM. Measuring radiation in space with bubble detectors and the effect of radiation on health system of human body. AIP Conference Proceedings, vol. 2839, AIP Publishing; 2023. https://doi.org/10.1063/5.0170939.
32. Hamdan M, Shehadeh M, Al Aboushi A, Hamdan A, Abdelhafez E. Photovoltaic Cooling Using Phase Change Material. Jordan Journal of Mechanical & Industrial Engineering 2018;12.
33. Arıcı M, Bilgin F, Nižetić S, Papadopoulos AM. Phase change material based cooling of photovoltaic panel: A simplified numerical model for the optimization of the phase change material layer and general economic evaluation. Journal of Cleaner Production 2018;189:738–45. https://doi.org/10.1016/j.jclepro.2018.04.057.
34. Rajput UJ, Yang J. Comparison of heat sink and water type PV/T collector for polycrystalline photovoltaic panel cooling. Renewable Energy 2018;116:479–91.

https://doi.org/10.1016/j.renene.2017.09.090.
35. Rustemli S, Dincer F. Modeling of photovoltaic panel and examining effects of temperature in Matlab/Simulink. Elektronika Ir Elektrotechnika 2011;3:35–40. https://doi.org/10.5755/j01.eee.109.3.166.
36. Potscavage WJ, Sharma A, Kippelen B. Critical interfaces in organic solar cells and their influence on the open-circuit voltage. Accounts of Chemical Research 2009;42:1758–67. https://doi.org/10.1021/ar900139v.
37. Sun Z, Yang Z. Improved maximum power point tracking algorithm with cuk converter for PV systems. The Journal of Engineering 2017;2017:1676–81. https://doi.org/10.1049/joe.2017.0617.
38. Dominguez J. Solar Energy Engineering Processes and Systems Second Edition. 2014.
39. Hamzah H, Toifur M, Ishafit I. Determination of Fill Factor and Efficiency in Solar Cell Type (99 × 69) mm2 with Arduino Uno R3 Based Drive assisted by Logger Pro 3.14.1. Indonesian Review of Physics 2019;2:53. https://doi.org/10.12928/irip.v2i2.1258.
40. Kant K, Shukla A, Sharma A, Biwole PH. Heat transfer studies of photovoltaic panel coupled with phase change material. Solar Energy 2016;140:151–61. https://doi.org/10.1016/j.solener.2016.11.006.
41. Xu Z, Kleinstreuer C. Concentration photovoltaic-thermal energy co-generation system using nanofluids for cooling and heating. Energy Conversion and Management 2014;87:504–12. https://doi.org/10.1016/j.enconman.2014.07.047.
42. Skoplaki E, Palyvos JA. On the temperature dependence of photovoltaic module electrical performance : A review of efficiency / power correlations. Solar Energy 2009;83:614–24. https://doi.org/10.1016/j.solener.2008.10.008.
43. Zhou J, Yi Q, Wang Y, Ye Z. ScienceDirect Temperature distribution of photovoltaic module based on finite element simulation. SOLAR ENERGY 2015;111:97–103. https://doi.org/10.1016/j.solener.2014.10.040.
44. Ahmed M, Radwan A. Performance evaluation of new modified low-concentrator polycrystalline silicon photovoltaic/thermal systems. Energy Conversion and Management 2017;149:593–607. https://doi.org/10.1016/j.enconman.2017.07.057.
45. Rejeb O, Sardarabadi M, Ménézo C, Passandideh-Fard M, Dhaou MH, Jemni A. Numerical and model validation of uncovered nanofluid sheet and tube type photovoltaic thermal solar system. Energy Conversion and Management 2016;110:367–77. https://doi.org/10.1016/j.enconman.2015.11.063.
46. Naumenko K, Eremeyev VA. A layer-wise theory for laminated glass and photovoltaic panels. Composite Structures 2014;112:283–91. https://doi.org/10.1016/j.compstruct.2014.02.009.
47. Emam M, Ahmed M. Cooling concentrator photovoltaic systems using various

configurations of phase-change material heat sinks. Energy Conversion and Management 2018;158:298–314. https://doi.org/10.1016/j.enconman.2017.12.077.

48. Hudișteanu SV, Țurcanu FE, Cherecheș NC, Popovici CG, Verdeș M, Ancaș DA, et al. Effect of Wind Direction and Velocity on PV Panels Cooling with Perforated Heat Sinks. Applied Sciences (Switzerland) 2022;12. https://doi.org/10.3390/app12199665.
49. Sarhaddi F, Farahat S, Ajam H, Behzadmehr A, Mahdavi Adeli M. An improved thermal and electrical model for a solar photovoltaic thermal (PV/T) air collector. Applied Energy 2010;87:2328–39. https://doi.org/10.1016/j.apenergy.2010.01.001.
50. Zainal Arifi, Suyitno Suyitno , Dominicus Danardono Dwi Prija Tjahjana, Wibawa Endra Juwana MRAP and ARP. The Effect of Heat Sink Properties on Solar Cell Cooling Systems. Applied Sciences 2020;10. https://doi.org/10.3390/app10217919.
51. Righetti G, Doretti L, Zilio C, Longo GA, Mancin S. Experimental investigation of phase change of medium/high temperature paraffin wax embedded in 3D periodic structure. International Journal of Thermofluids 2020;5–6:100035. https://doi.org/10.1016/j.ijft.2020.100035.
52. Shekoofa A, Emam Y, Pessarakli M. Effect of partial defoliation after silking stage on yield components of three grain maize hybrids under semi-arid conditions. Archives of Agronomy and Soil Science 2012;58:777–88.
53. Dmitruk A, Naplocha K, Grzęda J, Kaczmar JW. Aluminum inserts for enhancing heat transfer in PCM accumulator. Materials 2020;13. https://doi.org/10.3390/ma13020415.
54. Ranabhat K, Patrikeev L, Revina AA evna, Andrianov K, Lapshinsky V, Sofronova E. An introduction to solar cell technology. Journal of Applied Engineering Science 2016;14:481–91. https://doi.org/10.5937/jaes14-10879.